www.czasopisma.pan.pl PAN POLSKA AKADEMIA NAUK www.journals.pan.pl

Arch. Min. Sci. **67** (2022), 2, 275-287

Electronic version (in color) of this paper is available: http://mining.archives.pl

DOI: https://doi.org/10.24425/ams.2022.141458

TÜMAY KADAKCI KOCA[1*]

A CONCEPTUAL SECTOR-SCALE NUMERICAL MODELING OF A LANDSLIDE IN AN OPEN PIT MINE

In this study, an old rotational landslide that has reactivated in the NW sector of an open-pit mine operated within the gneiss rock unit was evaluated for geological and hydrogeological properties. The pit slopes were susceptible to mass movement when there were variations in water inflows. Considering this fact, a conceptual numerical model concerning geostructural features, rainfall infiltration, and varying hydrological conditions was constructed. Initially, finite element (FE) groundwater seepage analyses were performed to evaluate the effect of water flow on stability in the dry and rainy seasons. The rainy season was simulated by vertical infiltration. Since the dewatering measures are of importance in open pit slope instability mitigation, pumping wells were designed to control water flow through the disturbed zone to improve the stability of the sector that can be triggered again with changing environmental conditions. The performance and organization of the pumping wells were also simulated in the FE model. This FE model was part of a dewatering plan. From this, the effect of the pumping rate from the wells on the stability of the sector was revealed. It was also found that there should be an increase in the pumping rate in the rainy season.

Keywords: open pit mine; landslide; finite element; groundwater seepage analysis; pumping rate

1. Introduction

The geostructural features in an open-pit mine play a crucial role in the open pit slope design [1,2]. They control the water flow into the rock mass, whilst wide shear zones lead to the formation of concerning materials that have complex geological and hydrogeological properties. Hence, it is difficult to provide the stability of the overall slopes taking place in the fault zones. Long-term slope stability in open pits can only be achieved by providing full water drainage.

[1] MUĞLA SITKI KOÇMAN UNIVERSITY, TURKEY

* Corresponding author: tumaykoca@gmail.com

On the other hand, very weak rock layers are also assumed to be another controlling factor in pit slope design [3]. Hence, one can profit from the speed and ease of application of continuum methods. It is practical for most applications, and in the case of employing an accurate geological and hydrogeological model, many failure mechanisms can be captured by continuum modelling. Modern highly fractured rock slopes have been simulated in continuum modelling in slope stability assessment studies [4-13]. In addition, geostructural features such as faults, joints, foliation, and bedding planes can also be simulated in continuum codes depending on the scale of the engineering problem. Previous studies have studied incorporating the joints into the continuum models [4,8,14,15]. In addition, the precise engineering geological model requires a conceptual hydrogeological model as well as geological and rock mass behaviour modelling.

Except for the intrinsic hydrological conditions, rainfall infiltration and continuous rainfalls are the main triggers of landslides on both natural and engineered slopes [16-19]. Extreme rainfalls during a short time may not totally infiltrate and cause run-off. Run-off affects both the weathering process and the stability of rock masses. Rainfall infiltration leads to a rise in groundwater level (GWL) and pore water pressure, thus reducing the effective stress and the shear strength of earth material that may result in rainfall-induced slope failures [20]. In the literature, soil slopes have been investigated, considering the effect of rainfall more than rock slopes [21-28]. On the other hand, a small number of studies have investigated the rainfall effect on rock slope stability from different aspects, such as water weakening in the rock mass [18-20].

The dewatering wells as a component of the dewatering plan are vital in permanent open pit design [29,30]. Nevertheless, numerical simulation of dewatering wells in open-pit mines as a drainage measure has not been studied yet. For this reason, this study aims to perform a FE modelling to simulate the effect of pumping rate in dewatering wells on the stability of the slope. The variations in pumping rate depending on the dry and rainy season were also investigated, assuming vertical rainfall infiltration. For this purpose, a reactivated landslide in a sector of an open-pit mine was evaluated by the deterministic approach with the aid of a geological and conceptual hydrogeological model.

2. Geological and hydrogeological properties of the landslide

In the open pit, exposed gneiss, albite ore and mica veins/mica schists are found. The main geostructural features of the mine are the two strike-slip faults trending in the N45W direction. The width of this zone is approximately 60 m (Fig. 1). A landslide affecting the five benches has occurred. The landslide morphology indicates multiple landslides [31], such as a repeated development of the same type of movement occurring within the main landslide body. Hence, the reactivated zone within the main landslide body was termed the secondary failure. The main scarp is under the haul road at an elevation of 531 m. The secondary scarp is indeed the reactivation of the main landslide body starting from the 490 m elevation. The heavily jointed, disturbed, and highly weathered rock mass located between the elevations of 490 m and 460 m moved downslope while this section has a 26° slope angle. Even though the current overall slope angle is about 16°-18° from 490 m to the toe of the landslide, some benches naturally formed after the main landslide having slope angles higher than 30°.

Lateral and vertical displacements on the scarp of the secondary landslide were measured as ≥2.0 m and 1.0-1.5 m, respectively. The fundamental factors controlling the landslide are old

stream beds and the high permeability of disturbed material formed due to the tectonic deformation and the old landslide activity.

Based upon the analysis and interpretation of the structural data, the most dominant of the two discontinuity sets were defined. The 70° dipping to the NW joint set works as a back scarp of the landslide, whereas the steeply dipping (82°) joint set strikes approximately NW-SE with spacing between 62 cm and 78 cm forming the lateral release surfaces. On the other hand, foliation planes strike approximately NE-SW, dipping in the range between 34° to 36° to NW and have spacing between 5 cm and 25 cm.

On the upper bench of the toe part of the landslide (460 m), damp areas and a pond were observed in the field. The presence of a pond indicated that the water is leaking from the stream beds at higher elevations and carried into the failure area by discontinuities. In other words, water follows the path along the joints and flows into the landslide area. The damp areas at the elevations of 460 m also indicated that the toe of the landslide is under a wet zone and that the drained shear strength conditions exist at the base of the landslide. In addition, surface waters have been carried out by the creeks with the following directions of NNW to the pit base, and they are recharging the groundwater (Fig. 1). In the above perspective, the toe of the landslide will stay very close to the GWL in rainy seasons.

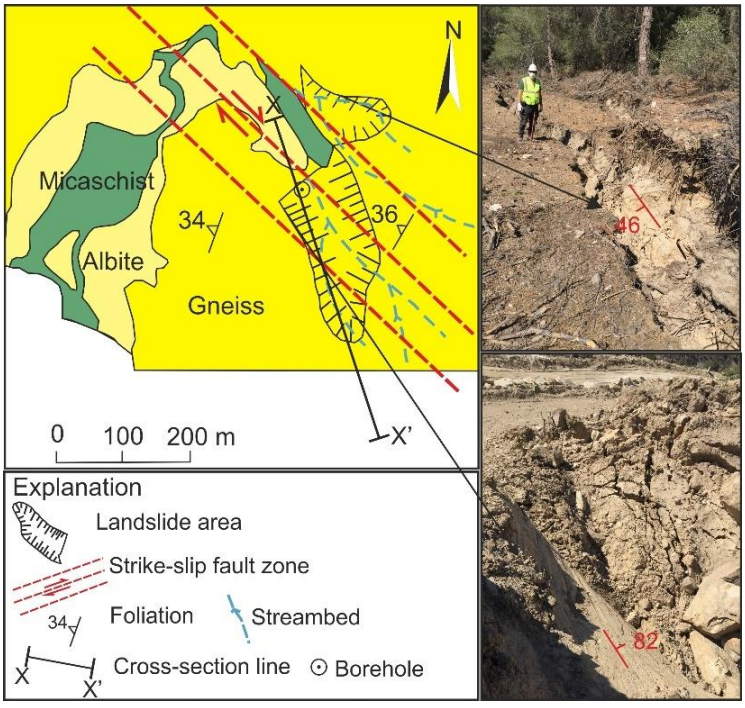

Fig. 1. Geological map of the landslide area and field-view of landslides

A very disturbed zone (RQD = 0%) was intersected at 2 to 5 m depth along the borehole drilled at the toe of the slope. Following this zone, a relatively harder gneiss unit with RQD values

between 64% and 84% was intersected. This finding supported the idea that the slip circle of the landslide could not pass through the hard gneiss unit located at the toe of the landslide, and hence the slip surface has daylighted at the toe (Fig. 1).

3. Climate

Heavy rainfall is frequently declared as the main trigger for slope instability [32-35]. The infiltration of rainfall water elevates the free surface of the groundwater in the slope and hence weakens the rock and soil at the potential slip surface, thus reducing the stability of the slope [35]. Since the upper disturbed and weathered (EWD) gneiss zone is highly permeable when compared to the underlying gneiss layers, the high-intensity rainfalls in a short time are of interest as a triggering factor rather than cumulative rainfall. On the other hand, a deep-seated landslide may be triggered by a cumulative rainfall effect. The maximum daily precipitation recorded between 2007 and 2020 is 93.8 mm; the monthly precipitation is above 110 mm in December and January [36].

4. Rock mass behaviour and FE model

Heavily fractured and highly weathered rock slopes can be assumed to obey the equivalent continuum, which considers isotropic and homogeneous media [37]. In this study, the stability investigation of the landslide was performed by the 2D FE method in conjunction with the shear strength reduction technique along a cross-section (Fig. 1), cutting the main and secondary mass movements to obtain a factor of safety value (SRF). An elastic-perfectly plastic behaviour can be readily used for faulted, densely fractured, and disturbed rock mass that reaches its residual strength values [38]. For this reason, elastic-perfectly plastic material behaviour for moderately to extremely weathered and disturbed gneiss units was used by considering the Generalized Hoek-Brown Criterion [37]. On the other hand, the mechanical behaviours of mica schist and road fill material were represented by the Mohr-Coulomb Criterion. As the discontinuity sets play an essential role in forming the lateral release surfaces and back scarp of the landslide body, discontinuities were simulated as structural elements between continuum bodies and represented as Mohr-Coulomb joints. The typical values of physical, mechanical, and deformation properties of the lithological units and joints used in the numerical analyses are given in Table 1.

A non-associated flow rule (dilation parameter = 0, no volume change) was considered. Boundary limit conditions were extended to the lateral and vertical sides until the numerical solutions were not significantly affected by the limits of the model. The mesh configuration was set to six noded, graded triangular elements. For the verification of the mesh size, several trial-and-error cycles for various mesh sizes were made until the results became insensitive to the number of elements used for the analysis [39-42]. The contiguity and quality of the mesh elements were checked based on the aspect ratio and orthogonality of the elements. A total of 8 bad elements out of 10679 were detected, and they were corrected by slightly modifying the boundaries and deleting the unnecessary vertices. After all, the simulated distance between consecutive nodes which affects the precision and duration of the calculations is changing between 0.5 m near the ground surface and 4.0 m at deeper elevations.

TABLE 1

Material and joint properties used in numerical analyses

Properties	MW-Gneiss	EWD-Gneiss	Ore (Albite)	Properties	Mica Schist	Road fill	Joints
	Generalized Hoek-Brown Criterion				Mohr-Coulomb Criterion		
© (kN/m^3)	26	18	27	© (kN/m^3)	22	18	
σ_{ci} (MPa)	27.34	1.50	72	σ_t (MPa)	5.86e^{-5}	0	0
σ_t (MPa)	0.007	2.29e^{-4}	0.027	c (MPa)	0.020	0.15	0.03
m_b	0.826	0.256	1.923	Φ (°)	26	35	21
s	0.0002	3.92e^{-5}	7e^{-4}	E_m (MPa)	130	25	
a	0.510	0.522	0.506	υ	0.30	0.25	
E_m (MPa)	2188.28	53.945	5364.09	k_n (GPa/m)			100
υ	0.25	0.30	0.25	k_n (GPa/m)			10

k_n: normal stiffness, k_s: shear stiffness; EWD: extremely weathered and disturbed, MW: Moderately weathered; σ_{ci}: UCS value of intact rock, σ_t: tensile strength, ©: unit weight, m_b, s, a: Hoek-Brown's constants, c: cohesion, Φ: internal friction angle, E_m: elastic modulus of rock mass, υ: Poisson's ratio (adapted from [43-44])

5. FE groundwater seepage analyses for dry conditions

For many pit slopes, the general direction of groundwater flow is from the crest of the slope to the toe [30]. However, the geostructural features significantly affect the groundwater flow. For this reason, the joint system consisting of 70° dipping joints and the foliation planes dipping towards the slope face with an angle of 34° were modeled as forming a block. Since the foliation planes are aligned perpendicular to the joint and fault zones, this position creates hydraulic barriers to vertical drainage and flow towards the pit face. The geological and conceptual hydrogeological model used in FE simulation is given in Fig. 2.

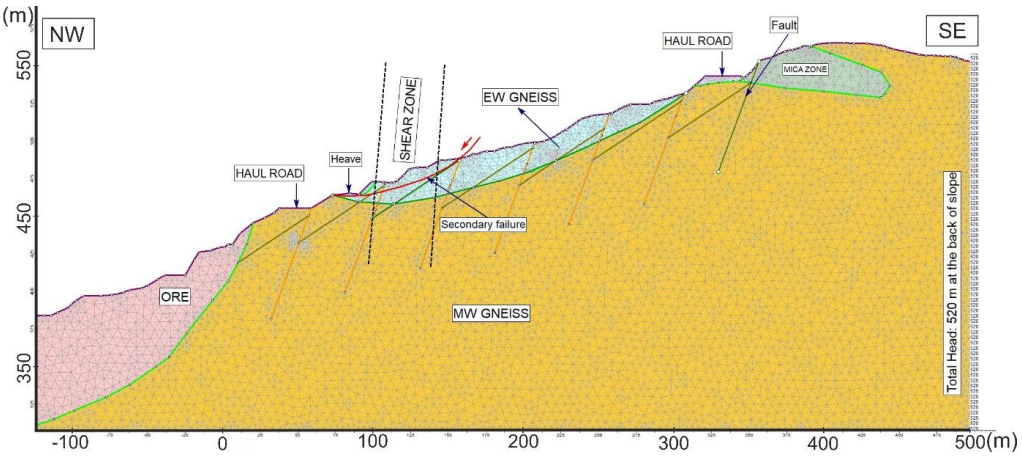

Fig. 2. The geological and conceptual hydrogeological model

In order to evaluate the long-term effect of water flow on stability, initially, FE steady-state groundwater seepage analyses were performed. Effective stresses were assumed during the analysis. The FE groundwater analysis was also employed to estimate the piezometric line for the dry season. The total head was assumed to be 520 m at the back of the slope according to the water seepage points observed in the field (Fig. 2).

It was thought that the weathered and disturbed rock material within the main landside gained an increased porosity and permeability, which hence led to reduced pore pressure. For a conservative design, the silty granular disturbed layer was modelled concerning the Fredlund-Xing permeability function [45].

$$K = K_s \frac{1}{\left[\ln \ln \left(e + \left(\frac{\psi}{A} \right)^B \right) \right]^C} \tag{1}$$

Where A, B, and C are the model parameters; e is 2.7182818; ψ is matric suction; K is permeability (m/s), and K_s is saturated permeability (m/s). The permeability coefficients of the underlying geological units were introduced into the numerical model as 10^{-7} m/s without a directional variation.

The simulation of the dry season was based on the total head (maximum GWL) of 520 m at the back of the slope. The discharge rates in the dry season are 2.537×10^{-8} m^3/s on average. The water flow model confirmed that the water flows towards the toe of the landslide body. On the other hand, the pore pressure under dry conditions shows a negative pore pressure zone indicating a capillarity above the GWL.

5.1. Simulation of rainfall effect on discharge rates

Rainfall infiltration is defined as the actual water amount in a rainfall process through the unit area of the surface per unit time [46]. The infiltration rate mainly depends on the soil type, soil structure, amount of aggregation, and soil water content [47]. If the rainfall infiltration rate of the weathered and disturbed layer is lower than the rainfall intensity, there will be a surface run-off, otherwise, the infiltrated rainfall water will recharge the groundwater. In this study, the evaluation of this relationship provided sight to how to simulate the GWL in deterministic analyses. It should be noted that the steady-state seepage conditions may turn into transient flow during the rainfall event. As the infiltration of rainfall in the heavily jointed and weathered rock mass, the transition from unsaturated to saturated conditions will simultaneously change the physical and mechanical properties of the rock mass. However, this study investigates the rainfall effect from a long-term stability point of view.

The effect of rainfall infiltration of the upper rock layer was simulated using the infiltration rate of 2.5×10^{-5} m/s. It means that a water layer of approximately 90 mm on the ground surface will be infiltrated in one hour. It corresponds to a moderately rapid infiltration according to Alvarez and Perelman [48]. This rate was applied to the disturbed and weathered section of the slope.

The results of the FE groundwater seepage analyses showed that after heavy rainfalls, the surface flow will occur. In addition, infiltration of rainwater along the pathways such as open joints, tension crack, and by the extremely weathered and disturbed material itself will contribute to instability due to the exerted discharge pressure in favour of driving forces. The mentioned

discharge rate along the main slip surface and joints in the rainy season was found to be changing between 0.571×10^{-5} and 1.008×10^{-5} m^3/s which is far more than in the dry season. When the discharged and infiltrated water is compared, the percentage of infiltrated rainwater was estimated to be 40%, while 60% of the rainwater turns into a surface flow. It is also seen from Fig. 3 that flow lines are strongly affected by the structural geometry and depend on the differential permeability of the ground (for example, follows the discontinuities or the contact between high and low permeable layers). The water mainly follows the joint and foliation planes and causes run-off for fully saturated conditions. Hence the preferential flow right after the rainfall does not allow infiltration to be very deep, subsequently, a portion of the infiltrated rainwater will be discharged at the lower part of the landslide area or the toe.

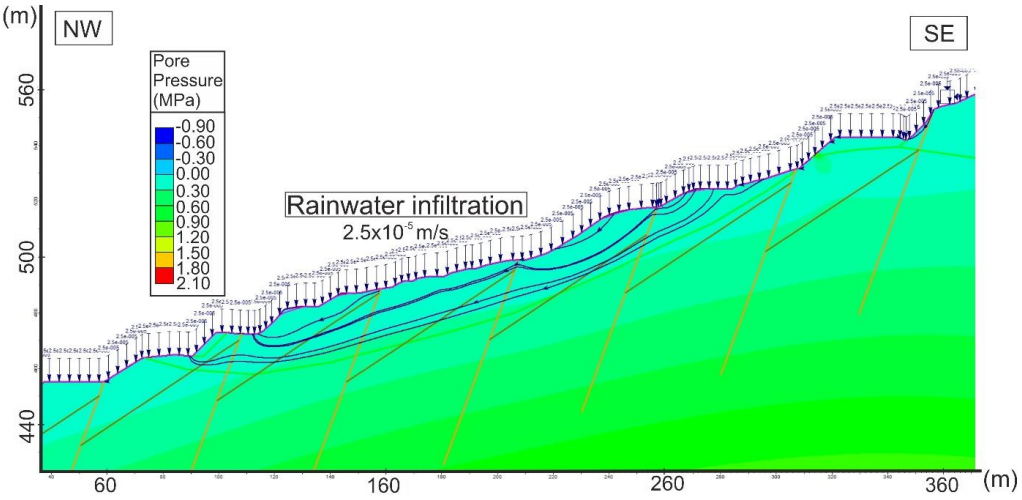

Fig. 3. The results of FE groundwater seepage analyses, distribution of pore pressure, and flow lines under rainfall infiltration

6. Deterministic analyses

As the capillarity between 460 m and 490 m, the disturbed material has a high degree of water saturation even during the dry season. The GWL obtained from FE groundwater seepage analysis was employed in the deterministic analyses of dry conditions. Except for the estimated static GWL, ponded water levels are expected during the rainy season. It means that the weathered and disturbed material is at a critical state in the dry period at an 18° of slope angle. However, it is noteworthy that rainfall events tend to bring the slope into failure. For this reason, the GWL was raised from 479 m to 491 m at the upper slope to represent the phreatic line in the rainy season, similarly applied by Kafle et al. [49]. It allowed us to investigate the worst conditions for rainfall infiltration and probable capillarity acting on the disturbed material lying over the GWL.

The dry and saturated (rainy season) models yielded SRF of 1.31 and 1.10, respectively (Fig. 4a,b). The maximum shear strain contours were detected to be starting from the elevation of 525 m and following the main slip surface, whereas the secondary failure zone is likely to

be unaffected by the shear failures. This result supported the idea that the disturbed material is discharged more rapidly than the underlying less permeable MW gneiss unit, hence the main slip surface is under threat of reactivation in changing hydrological and environmental conditions (Fig. 4).

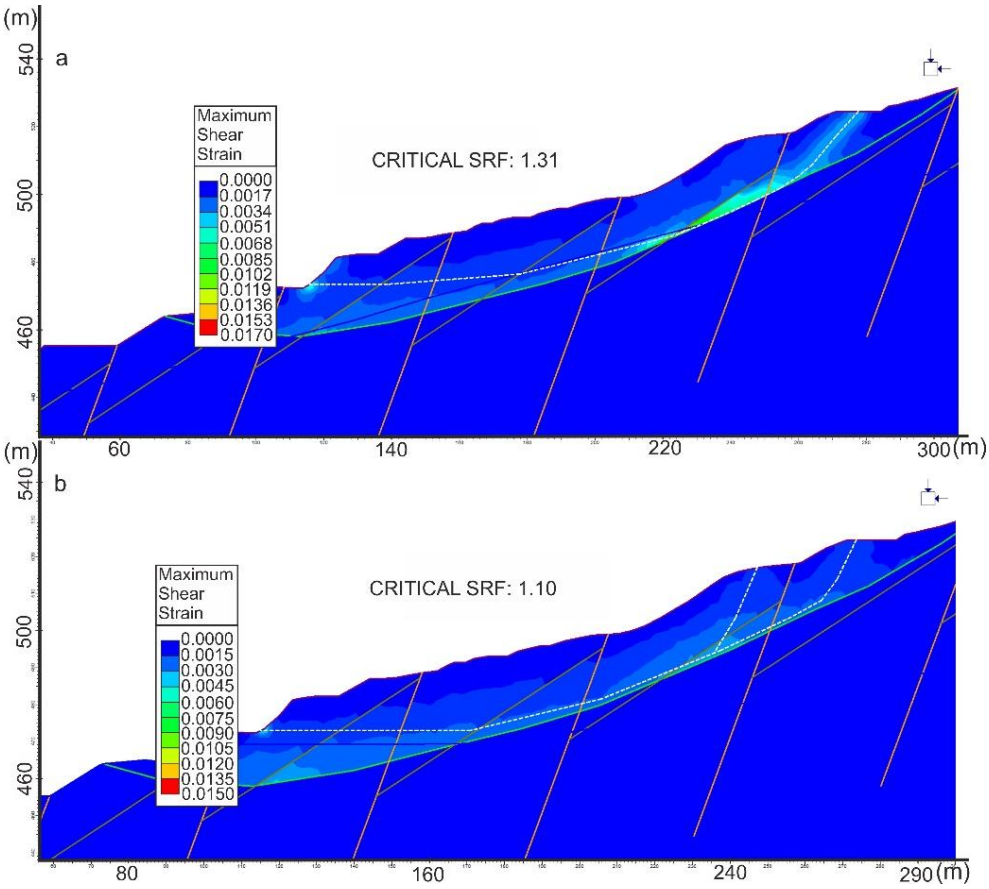

Fig. 4. Maximum shear strain contours of a) dry model b) saturated model (dashed lines are the estimated failure planes)

7. Simulation of drainage measures

As a consequence of the deterministic analyses, a concurrent dewatering plan is required for the NE sector of the open pit. The dewatering plan may involve pumping from vertical wells. The goal of the pumping well is to reduce the pore pressures right above and under the boundary of EWD and MW gneiss (main slip surface) and to reduce the inward hydraulic gradient into the pit. As a result, groundwater inflow to operating areas is permitted. The four vertical pumping wells starting at the elevation of 500 m at the surface from north to south can be planned

at a 15 m distance from each other. The wells can be installed until the depth of 25 m from the ground surface which crosses the extremely disturbed zone. However, the structural orientation exerts anisotropy to the permeability as which the flow can be oblique to the hydraulic gradient by following the plane of the fault zone. The design of four wells in the north-south direction is given in Fig. 5. The pumping rate along the wells was simulated as negative vertical infiltration along the well as a discharge section. In this manner, the discharge sections as pumping wells were inserted into the model to observe the flow rates, and the boundary conditions were set as negative vertical infiltration at the top of the wells to represent the pumping effect.

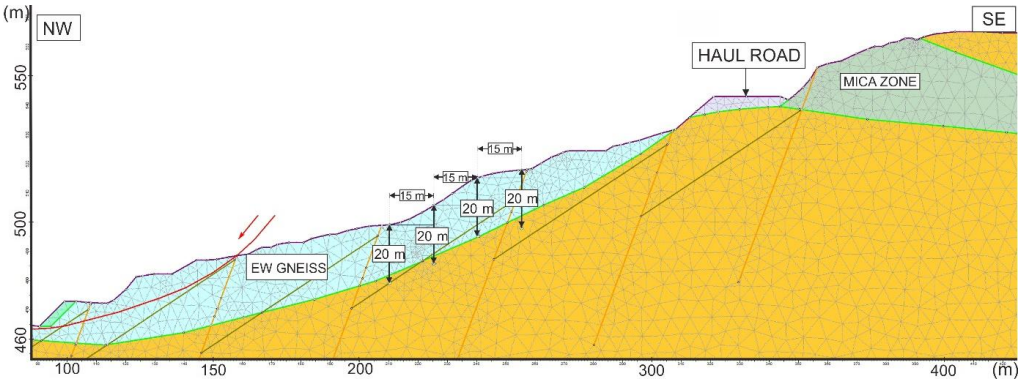

Fig. 5. Design of discharge sections to pump water out of the slope

The elevation of 500 m was chosen in particular for the well location since the deterministic FE models showed that maximum shear strain contours were concentrated under this elevation on the main slip surface.

A trial set of hydrological models concerning different pumping rates was calculated until an appropriate pumping rate was reached. The appropriate pumping rate refers to the optimum rate at which the flow lines do not saturate the weathered and disturbed material and do not exaggerate the negative pore pressure within the disturbed material. In other words, if the pumping rate is high, negative pore pressures develop. On the other hand, if the pumping rate is low, water still saturates the disturbed zone, flows towards the toe of the landslide and the GWL is not reduced.

The results for the dry season indicated that the flow rate is approximately 1.51×10^{-7} m^3/s across the discharge section to the base of the open pit. The total discharge velocity at the bottom of the wells is also showing deficient rates such as 5.84×10^{-10} m/s. These values indicate that pumping wells significantly decreased the flow rate and velocity towards the open pit base. For these reasons, an optimum pumping rate of 1.25×10^{-6} m/s can be chosen. If a higher pumping rate than the optimum pumping rate is used, the pore pressures will excessively increase. The SRF increased to 1.37 for dry conditions when the pumping well is operated (Fig. 6a). In addition to the slightly improved SRF value, total displacement along the estimated failure surface decreased to 2.5 cm. It is also indicated from Fig. 6a that the groundwater level (pink line) was successfully lowered below the disturbed material with the water pumping, and fewer flow vectors are observed within the landslide area. 1.25×10^{-6} m/s pumping rate from the wells was

also tested for the rainy season. However, it was observed that the water still percolated into the landslide body and the flow continued towards the toe of the slope. Subsequently, a 1.25×10^{-2} m/s pumping rate was employed for the saturated model, and the SRF increased to 1.35 for saturated (rainy) conditions (Fig. 6b). Not only did SRF increase, but also the detected total displacement along maximum shear strain zones decreased to 8 cm. It was also observed from Fig. 6a that, under heavy rainfall, the applied pumping rate prevented surface flow, and the groundwater level decreased within the landslide area. The pore pressures were found to be changing between –1.20 MPa above the GWL and 0.19 MPa in the extremely disturbed zone. This result showed that the pumping rate from the wells should be increased in the rainy season. However, the site response to the pumping needs to be observed and evaluated. Otherwise, high pumping rates may cause enormous negative pore pressures. In this context, piezometers can be placed to monitor the changes in the pore pressure in the field.

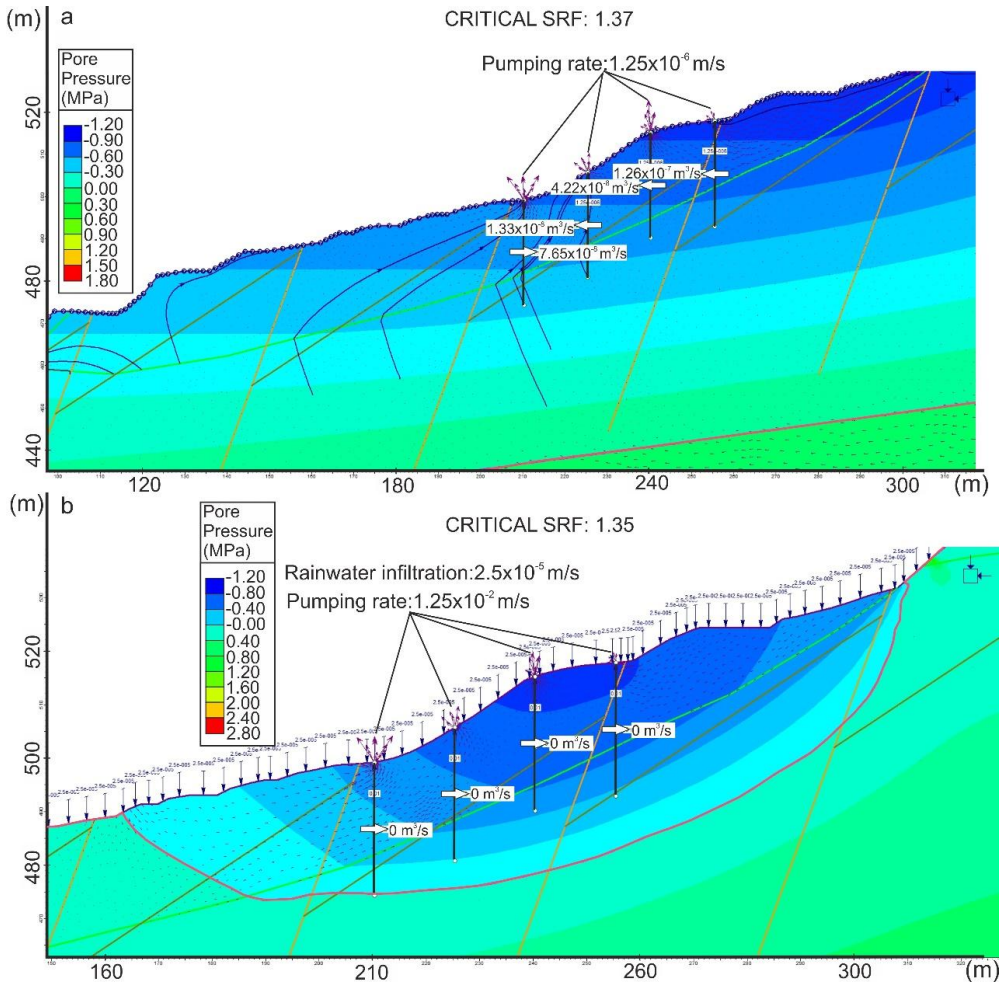

Fig. 6. Pore pressure distribution under an optimum pumping rate a) dry season b) rainy season

8. Conclusions

In this study, a conceptual sector-scale numerical modelling of a reactivated landslide in an open-pit mine was performed considering the rainfall effect and hydrogeological conditions. Even though numerical modelling of fractured and weak rocks considering the joints, hydrogeological conditions, and rainfall infiltration has been extensively worked on in the literature, the simulation of dewatering measures such as pumping wells in open-pit mines has not been studied yet. In the context of numerical modelling, initially, FE groundwater seepage analyses were performed. These analyses revealed the effect of rainfall infiltration on the discharge rates along joints as well as the approximate location of static GWL. The increase in water flow rate and velocity towards the toe of the landslide area was pronounced in the rainy season as expected. Subsequently, the calculated groundwater conditions were imported to the models for deterministic slope stability assessment to derive SRF values. The effect of rainfall was also simulated by increasing the GWL in saturated deterministic models. The maximum shear strain contours reaching the slope surface for the rainy condition highlighted a requirement for a dewatering plan on the slope. Hence, the reactivated secondary failure should be due to similar reasons that triggered the initial old landslide, such as the accumulation of water within the landslide body. The disturbed and weathered material is highly permeable, whereas the underlying MW gneiss is relatively less permeable. In addition, the perpendicularly aligned joints and foliation planes inclined towards the base of the pit may provide perched water levels. For these reasons, pore pressure and discharge pressure in the direction of failure may occur. Hence, pumping wells were designed at the elevations where the maximum shear strain contours were initiated. Trial sets of pumping rates were tested to keep the GWL below the extremely weathered and disturbed material zone whilst increasing the critical SRF value and decreasing the amount of total displacement. The simulations of several pumping rates provided optimum pumping rates for dry and rainy seasons. 1.25×10^{-6} m/s and 1.25×10^{-2} m/s pumping rates were determined for the dry model and saturated model under a rainfall infiltration of 2.5×10^{-5} m/s, respectively. However, while the dewatering plan is operated in the pit, a further transient flow simulation is required with the simultaneously derived piezometric data. Hence, the pumping rate can be improved depending on the variability of the hydrogeological data over time.

References

[1] D.R. Piteau, Geological factors significant to the stability of slopes cut in rock. In: P.W.J. van Rensburg (Ed.) Planning Open Pit Mines Proceedings of the Symposium on the Theoretical Background to the Planning of Open Pit Mines with Special References to Slope Stability 1970, Balkema (1971).

[2] D.C. Wyllie, C.W. Mah, Rock Slope Engineering Civil and Mining, Spon. Press, New York (2004).

[3] J. Read, P. Stacey, Guidelines for Open Pit Slope Design. CRC Press/Balkema, Leiden, Netherlands (2009).

[4] R.E. Hammah, J.H. Curran, T.E. Yacoub, B. Corkum, Stability analysis of rock slopes using the finite element method. In: Proceedings of the ISRM Regional Symposium EUROCK 2004 and the 53rd Geomechanics Colloquy, Salzburg, Austria (2004).

[5] R.E. Hammah, T.E. Yacoub, B. Corkum, J.H.A. Curran, The shear strength reduction method for the Generalized Hoek-Brown Criterion. In: Proceedings of 40th U.S. Symposium on Rock Mechanics 2005, Alaska (2005a).

[6] R.E. Hammah, T.E. Yacoub, B. Corkum, J.H.A. Curran, Comparison of finite element slope stability analysis with conventional limit-equilibrium investigation. In: Proceedings of 58th Canadian Geotechnical and 6th Joint IAH-CNC and CGS Groundwater Specialty Conferences 2005, Canada (2005b).

[7] A.J. Li, R.S. Merifield, A.V. Lyamin, Stability Charts for Rock Slopes Based on The Hoek-Brown Failure Criterion. Int. J. Rock Mech. Min. Sci. **45** (5), 689-700 (2008). DOI: https://doi.org/10.1016/j.ijrmms.2007.08.010

[8] A. Azami, T. Yacoub, J. Curran, D. Wai, A constitutive model for jointed rock mass. In: Proceedings of International Society for Rock Mechanics and Rock Engineering (ISRM) Symposium (EUROCK) 2013, Wroclaw, Poland (2013).

[9] R. Singh, R.K. Umrao, T.N. Singh, Stability Evaluation of Road-Cut Slopes in the Lesser Himalaya of Uttarakhand, India: Conventional and Numerical Approaches. Bull. Eng. Geol. Environ. **73** (3), 845-857 (2014). DOI: https://doi.org/10.1007/s10064-013-0532-1

[10] C.W. Sun, J.R. Chai, Z.G. Xu, Y. Qin, X.Z. Chen, Stability Charts for Rock Mass Slopes Based on the Hoek-Brown Strength Reduction Technique. Eng. Geol. **214**, 94-106 (2016). DOI: https://doi.org/10.1016/j.enggeo.2016.09.017

[11] C.K. Aswathi, A. Jana, A. Dey, S. Sreedeep, Stability assessment of a heavily jointed rock slope using limit equilibrium and finite element methods. In: Proceedings of Indian Geotechnical Conference (GeoNEst) 2017, Guwahati, India (2017).

[12] S.P. Pradhan, T. Siddique, Stability Assessment of Landslide-Prone Road Cut Rock Slopes in Himalayan Terrain: A Finite Element Method Based Approach. J. Rock Mech. Geotech. Eng. **12** (1), 59-73 (2020). DOI: https://doi.org/10.1016/j.jrmge.2018.12.018

[13] S. Sarkar, K. Pandit, N. Dahiya, P. Chandna, Quantified Landslide Hazard Assessment Based on Finite Element Slope Stability Analysis for Uttarkashi – Gangnani Highway in Indian Himalayas. Nat Hazards **106**, 1895-1914 (2021). DOI: https://doi.org/10.1007/s11069-021-04518-x

[14] R.E. Hammah, T.E. Yacoub, B. Corkum, F. Wibowo, J.H. Curran, Analysis of blocky rock slopes with finite element shear strength reduction analysis. In: Proceedings of 1st Canada – U.S. Rock Mechanics Symposium 2007, Vancouver, Canada (2007).

[15] M. Abdulai, M. Sharifzadeh, Uncertainty and Reliability Analysis of Open Pit Rock Slopes: A Critical Review of Methods of Analysis. Geotech. Geol. Eng. **37**, 1223-1247 (2019). DOI: https://doi.org/37.10.1007/s10706-018-0680-y

[16] P.J. Vardon, Climatic Influence on Geotechnical Infrastructure: A Review. Environ. Geotechn. **2** (3), 166-174 (2015). DOI: https://doi.org/10.1680/envgeo.13.00055

[17] K. Martinović, K. Gavin, C. Reale, C. Mangan, Rainfall Thresholds as a Landslide Indicator for Engineered Slopes on the Irish Rail Network. Geomorphology **306**, 40-50 (2018). DOI: https://doi.org/10.1016/j.geomorph.2018.01.006

[18] Y. Pan, G. Wu, Z. Zhao, L. He, Analysis of Rock Slope Stability Under Rainfall Conditions Considering the Water-Induced Weakening of Rock. Comput. Geotech. **128**, 103806 (2020). DOI: https://doi.org/10.1016/j.compgeo.2020.103806

[19] Q. Li, Y.M. Wang, K.B. Zhang, H. Yu, Z.Y. Tao, Field investigation and numerical study of a siltstone slope instability induced by excavation and rainfall. Landslides **17**, 1485-1499 (2020). DOI: https://doi.org/10.1007/s10346-020-01396-5

[20] T. Kadakci Koca, PhD thesis, Multi-Temporal Stability Investigation of Landslides in Çağlayan Dam Reservoir Area. Dokuz Eylül University, İzmir, Turkey (2021).

[21] F. Cai, K. Ugai, Numerical Analysis of Rainfall Effects on Slope Stability. Int. J. Geomech. **4** (2), 69-78 (2004). DOI: https://doi.org/10.1061/(ASCE)1532-3641(2004)4:2(69)

[22] S. Bai, J. Wang, B. Thiebes, C. Cheng, Y. Yang, Analysis of The Relationship of Landslide Occurrence with Rainfall: A Case Study of Wudu County, China. Arab. J. Geosci. **7** (4), 1277-1285 (2014). DOI: https://doi.org/10.1007/s12517-013-0939-9

[23] J. Beullens, D. Van de Velde, J. Nyssen, Impact of Slope Aspect on Hydrological Rainfall and on The Magnitude of Rill Erosion in Belgium and Northern France. Catena **114** (1), 129-139 (2014). DOI: https://doi.org/10.1016/j.catena.2013.10.016

[24] M. Rabie, Comparison Study Between Traditional and Finite Element Methods for Slopes Under Heavy Rainfall. HBRC J. **10** (2), 160-168 (2014). DOI: https://doi.org/10.1016/j.hbrcj.2013.10.002

[25] H. Dingiu, T. Zhigang, H. Zhenli, W. Jiamin, Numerical Analysis of Rainfall Saturated-Unsaturated Seepage and Stability of Expansive Soil Slope with Fissures. In: Proceedings of International Conference on Structural, Mechanical and Materials Engineering (ICSMME) 2015, Dalian, China (2015).

[26] R.C. Sidle, T.A. Bogaard, Dynamic Earth System and Ecological Controls of Rainfall-Initiated Landslides. Earth Sci. Rev. **159**, 275-291 (2016). DOI: https://doi.org/10.1016/j.earscirev.2016.05.013

[27] B. Wang, P.J. Vardon, M.A. Hicks, Rainfall-Induced Slope Collapse with Coupled Material Point Method. Eng. Geol. **239**, 1-12 (2018). DOI: https://doi.org/10.1016/j.enggeo.2018.02.007

[28] F.K. Rengers, L.A. McGuire, N.S. Oakley, J.W. Kean, D.M. Staley, H. Tang, Landslides After Wildfire: Initiation, Magnitude, and Mobility. Landslides **17**, 2631-2641 (2020). DOI: https://doi.org/10.1007/s10346-020-01506-3

[29] L.C. Atkinson, The role and mitigation of groundwater in slope stability, in: Hustrulid et al. (Eds.), Slope Stability in Surface Mining, Littleton, Colorado, USA (1998).

[30] G. Beale, J. Read, Guidelines for Evaluating Water in Pit Slope Stability, CRC Press/Balkema, Leiden, Netherlands (2013).

[31] International Association of Engineering Geology (IAEG) Commission on Landslides, Suggested Nomenclature for Landslides, Bull. Int. Assoc. Eng. Geol. **41** (1), 13-16 (1990). DOI: https://doi.org/10.1007/BF02590202

[32] C. Tang, J. Zhu, W.L. Li, J.T. Liang, Rainfall-triggered Debris Flows Following the Wenchuan Earthquake. Bull. Eng. Geol. Environ. **68**, 187-194 (2009). DOI: https://doi.org/10.1007/s10064-009-0201-6

[33] S. Kimoto, F. Oka, E. García, Numerical Simulation of the Rainfall Infiltration on Unsaturated Soil Slope Considering a Seepage Flow. Geotech. Eng. J. SEAGS & AGSSEA **44** (3), 1-13 (2013).

[34] K. Sasahara, N. Sakai, Shear and Compression Strain Development in Sandy Model Slope Under Repeated Rainfall. Soils Found. **57** (6), 920-934 (2017). DOI: https://doi.org/10.1016/j.sandf.2017.08.021

[35] Y. Chen, G. Liu, N. Li, X. Du, S. Wang, R. Azzam, Stability evaluation of slope subjected to seismic effect combined with consequent rainfall. Eng. Geol. **266**, 105461 (2020). DOI: https://doi.org/10.1016/j.enggeo.2019.105461

[36] https://www.mgm.gov.tr/veridegerlendirme/il-ve-ilceler-istatistik.aspx?k=H&m=AYDIN accessed: 11.01.2022

[37] E. Hoek, C. Carranza-Torres, B. Corkum, Hoek-Brown Criterion-2002 edition, in: Proceedings of North American Rock Mechanics Symposium 2002, Canada (2002).

[38] T. Kadakci Koca, M.Y. Koca Comparative Analyses of Finite Element and Limit-Equilibrium Methods for Heavily Fractured Rock Slopes. J. Earth Syst. Sci. **129**, 49 (2020).

[39] D.P. Kanunga, A. Pain, S. Sharma Finite element modeling approach to assess the stability of debris and rock slopes: a case study from the Indian Himalayas. Nat. Hazards **69**, 1-24 (2013).
DOI: https://doi.org/10.1007/s11069-013-0680-4

[40] Y.M. Cheng, C.K. Lau Slope Stability Analysis and Stabilization; 2nd ed. CRC Press Taylor & Francis Group, New York (2014).

[41] V. Gupta, R.K. Bhasin, A.M. Kaynia, V. Kumar, A.S. Saini, R.S. Tandon, T. Pabst Finite element analysis of failed slope by shear strength reduction technique: a case study for Surabhi Resort Landslide, Mussoorie township, Garhwal Himalaya. Geomatics, Nat. Hazards Risk **7** (5), 1677-1690 (2016).
DOI: https://doi.org/10.1080/19475705.2015.1102778

[42] G.C. Komadja, S.P. Pradhan, A.R. Roul, B. Adebayo, J.B. Habinshuti, L.A. Glodji A.P. Onwualu Assessment of stability of a Himalayan road cut slope with varying degrees of weathering: A finite-element-model-based approach. Heliyon **6**, e05297 (2020). DOI: https://doi.org/10.1016/j.heliyon.2020.e05297

[43] T. Kadakci Koca, M.Y. Koca, Slope Stability Assessment of Rock Slopes in an Open Pit Albite Mine Using Finite Element Method (FEM), Geol. Eng. J. **38** (1), 1-17 (2014).

[44] S.D. Karagöz, M.Y. Koca, Monitoring of the Landslide Occurred in the Alipaşa Open-Pit Albite Mine by Using GPS and the Recognition of Causes of This Phenomenon. Geol. Eng. J. **40** (1), 27-52 (2016).

[45] D.G. Fredlund, A. Xing, Equations for the Soil-Water Characteristic Curve. Can. Geotech. J. **31**, 521-532 (1994). DOI: http://dx.doi.org/10.1139/t94-061

[46] G. Zhang, Y. Qian, Z. Wang, B. Zhao Analysis of Rainfall Infiltration Law in Unsaturated Soil Slope. Sci. World J. 2014, 567250 (2014). DOI: http://dx.doi.org/10.1155/2014/567250

[47] B. Lowery, M.A. Arshad, R. Lal, W.J. Hickey, Soil water parameters and soil quality, in: J.W. Doran, A.J. Jones (Eds.) Methods for assessing soil quality, Soil Sci. Soc. Am. Spec. Publ. 49. SSSA, Madison, WI (1996).

[48] C.R. Alvarez, S. Perelman, Topsoil Structure in No-Tilled Soils in the Rolling Pampa, Argentina. Soil Res. **52** (6), 533-542 (2014). DOI: https://doi.org/10.1071/SR13281

[49] L. Kafle, W. Xu, S. Zeng, T. Nagel, A Numerical Investigation of Slope Stability Influenced by The Combined Effects of Reservoir Water Level Fluctuations and Precipitation: A Case Study of The Bianjiazhai Landslide in China. Eng. Geol. **297**, 106508 (2022). DOI: https://doi.org/10.1016/j.enggeo.2021.106508